Journal of Physics D:
Applied Physics

PAPER

Controlling phase transitions in MnNiGe using thermal quenching and hydrostatic pressure

To cite this article: Jing-Han Chen *et al* 2024 *J. Phys. D: Appl. Phys.* **57** 205003

IOP Publishing Journal of Physics D: Applied Physics
J. Phys. D: Appl. Phys. **57** (2024) 205003 (10pp) https://doi.org/10.1088/1361-6463/ad297f

Controlling phase transitions in MnNiGe using thermal quenching and hydrostatic pressure

Jing-Han Chen[1,*], Tej Poudel Chhetri[1], Anthony T Grant[1], Xiaojian Bai[1], Qiang Zhang[2], Chung-Kai Chang[3], David P Young[1], Igor Dubenko[4], Saikat Talapatra[4], Naushad Ali[4] and Shane Stadler[1]

[1] Department of Physics and Astronomy, Louisiana State University, Baton Rouge, LA 70803, United States of America
[2] Neutron Scattering Division, Oak Ridge National Laboratory, Oak Ridge, TN 37831, United States of America
[3] National Synchrotron Radiation Research Center, Hsinchu 30076, Taiwan
[4] School of Physics and Applied Physics, Southern Illinois University, Carbondale, IL 62901, United States of America

E-mail: jhchen10@lsu.edu

Received 12 December 2023, revised 25 January 2024
Accepted for publication 14 February 2024
Published 26 February 2024

Abstract

The phase transitions in MnNiGe compounds were explored by manipulating the heat treatment conditions and through hydrostatic pressure application. As the quenching temperature increased, both the first-order martensitic structural transition temperatures and magnetic transition temperatures decreased relative to those in the slowly-cooled samples. When the samples were quenched from 1200 °C, the first-order martensitic structural transition temperature lowered by more than 200 K. The structural transitions also shifted to lower temperature with the application of hydrostatic pressure during measurement. Temperature-dependent x-ray diffraction results reveal that the changes of the cell parameters resulting from the structural transitions are nearly identical for all samples regardless of the extensive variation in their structural transition temperatures. In addition, neutron scattering measurements confirm the magnetic structure transition between simple and cycloidal spiral magnetic structures.

Keywords: material design, phase transition, high pressure magnetism

1. Introduction

Due to the need to develop energy-efficient and climate-friendly temperature control devices, the research of magnetic cooling applications and the associated materials exhibiting magnetocaloric effects have drawn increasing attention. On the one hand, the effort of searching for magnetic materials with giant magnetocaloric effects resulting from coupled magneto-structural phase transitions has grown [1–9]. On the other hand, an increasing effort has been put on understanding the causes of magnetic and structural phase transitions in many magnetic materials, including $Gd_5Si_xGe_{4-x}$ [10, 11], Ni–Mn-based full Heusler alloys [12–22], and intermetallic MnTX (T = transition metal and X = Ge) systems [23–26].

Among the materials mentioned above, intermetallic MnTX systems are of interest because their abrupt volume modifications across first-order martensitic structural transitions directly results in giant magnetocaloric and barocaloric effects. The current work focuses on MnNiGe, which crystallizes in

* Author to whom any correspondence should be addressed.

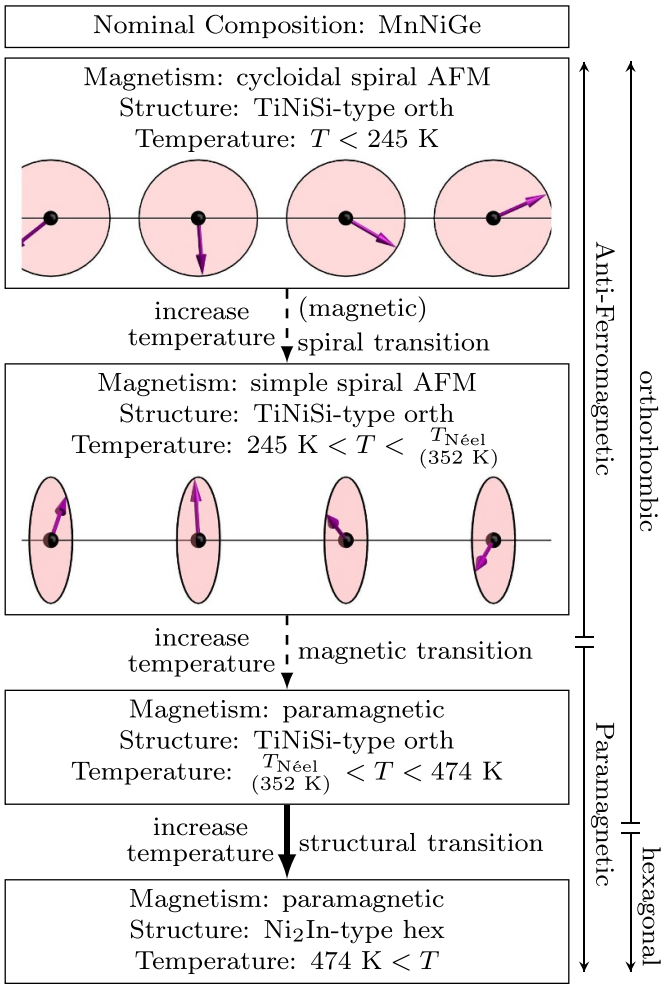

Figure 1. Progression of magnetic and structural phase transitions in MnNiGe samples prepared by slowly cooling after the melt.

a TiNiSi-type orthorhombic martensite phase (space group: *Pnma*) with a cycloidal spiral antiferromagnetic structure below 245 K. As the temperature increases above 245 K, its magnetic structure transforms to a simple spiral antiferromagnetic structure until it reaches its Néel temperature at 352 K. During this spiral magnetic transition, the direction of the propagation vector remains the same but the rotation plane of the magnetic elements change as illustrated in figure 1. As the temperature continues to increase, its crystal structure transforms from a TiNiSi-type orthorhombic martensite paramagnetic phase to a Ni_2In-type hexagonal austenite paramagnetic phase (space group: $P6_3/mmc$) above 474 K [25–27]. The progression of the magnetic and structural transitions is illustrated in figure 1.

Previous reports indicate that the magnetic transitions and martensitic structural transitions in MnNiGe can be controlled through substitution at the Mn [28–39], Ni [27, 33, 37, 40–45], or Ge [46–48] sites. Alternatively, stoichiometry modification [49], pressure application [24, 38, 44], or rapid solidification [50] can also affect the structural and magnetic phase transitions considerably without introducing other elements or even without modifying the composition. In addition, heat treatments have also been proven to be an effective way to modify the phase transitions, which has been demonstrated in similar materials such as $Mn_{1-x}Co_xNiGe$ [40, 41], MnCoGe [51], $(MnNiSi)_{0.65}(Fe_2Ge)_{0.35}$ [52], and $(MnNiSi)_{0.62}(FeCoGe)_{0.38}$ [53]. However, heat treatment methods and associated pressure-induced effects have not been investigated systematically in MnNiGe compounds, in which the magnetic and structural transitions are decoupled. It is known that the magnetostructural transitions often coincide with large magnetocaloric effects that can be exploited in magnetic cooling technologies. Therefore, the motivations for this study are centered on exploring the relationship between magnetic, structural, and/or magnetostructural transitions near room temperature in MnNiGe through the application of thermal/quenching techniques and/or the application of hydrostatic pressure.

In the current work, MnNiGe samples were first synthesized by melting elemental Mn, Ni, and Ge together, and then portions of this source material were further processed through annealing, quenching, and/or slow-cooling. The properties of their phase transitions in response to temperature, hydrostatic pressure, and magnetic field were investigated. As a result, both magnetic and structural phase transitions were preserved in all the samples. However, increasing the quenching temperature drastically decreased the first-order martensitic structural transition temperature (>200 K) and decreased the magnetic transition temperatures to a lesser degree (<50 K). When the sample was quenched at 1200 °C, i.e. the upper temperature limit of the sealed quartz tubes used in this study, the lowest first-order martensitic structural transition temperature (329 K) was observed, whereas the highest one (474 K) occurred for the samples cooled slowly from 1100 °C at 30 °C h^{-1}. In addition, two of the samples with lower structural transitions were selected for temperature-dependent magnetization measurements under hydrostatic pressure application. As the hydrostatic pressure increased, the first-order martensitic structural transition temperatures decreased.

2. Sample preparation

The MnNiGe samples were prepared by weighing equiatomic amounts of high purity Mn (99.95%), Ni (99.95%), and Ge (99.999%) elements inside alumina crucibles, which were then sealed in quartz tubes under vacuum. The materials were then heated to 1100 °C and dwelled for 12 h. After naturally cooling down, they were crushed easily with an agate mortar and pestle. To promote the homogeneity of their chemical compositions, the crushed materials were heat treated again at 1100 °C for another 12 h, and then cooled from 1100 °C to room temperature at 30 °C h^{-1}. The resulting 30 g sample was labeled as SC1100, where 'SC' stands for 'slowly cooled', and served as the source ingot for preparing the other samples.

For different heat treatments, parts of the source sample were placed in alumina crucibles and then sealed in quartz tubes under vacuum. The samples were separately heated to 1000 °C, 1100 °C, and 1200 °C for 12 h (labeled as AQ1000, AQ1100, and AQ1200, respectively), and then quenched.

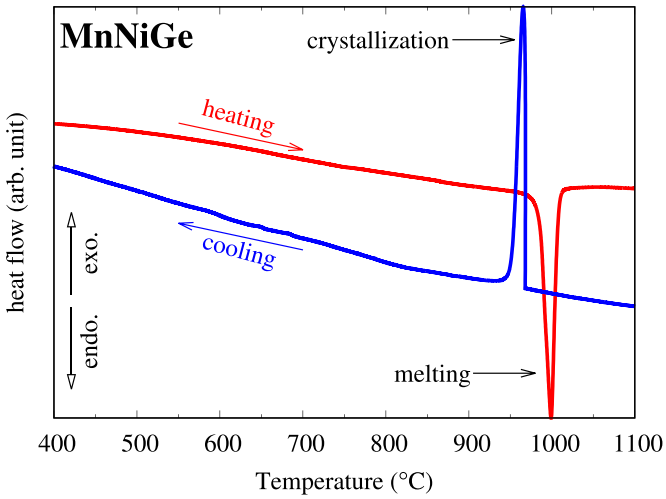

Figure 2. Heat flow results on MnNiGe. First-order phase transitions due to the melting/crystallization are observed between 900 °C and 1050 °C with thermal hysteresis.

Table 1. The heat treatment conditions of the samples and their corresponding properties.

Label	Heat treatment (°C)		Spiral trans.[a] (K)	Néel Temp.[a] $\mathbf{T_N}$ (K)	Struct.[b] trans. (K)	a (Å)	b (Å)	c (Å)	vol./f.u.[c] (Å^3)
SC1100	1100	(slowly cooled)	245	352	474	6.041	3.717	7.078	39.734
AQ1000	1000	(quenched)	235	349	400	6.026	3.720	7.067	39.605
AQ1100	1100	(quenched)	221	345	371	6.021	3.720	7.062	39.540
AQ1200	1200	(quenched)	200	—	329	6.015	3.719	7.055	39.457

[a] Magnetic phase transition temperatures were obtained from the magnetization experiments shown in figure 3.
[b] The first-order martensitic structural transition temperatures were extracted from the magnetization and calorimetric results shown in figure 3.
[c] The cell parameters, i.e. a, b, c, and volume, were estimated from powder diffraction experiments performed at 100 K and the results are shown in figure 7.

The heat treatment conditions of all the samples and their respective properties are summarized in table 1. These quenching processes have been commonly applied to metallic materials so that atomic disorder in their liquid configuration could be preserved at room temperature [54].

Composition analyses were performed using an Epsilon 3XLE, benchtop energy-dispersive x-ray fluorescence spectrometer manufactured by Malvern Panalytical Ltd The results reveal the composition to be $Mn_{32.3}Ni_{34.4}Ge_{33.1}$ for all the samples.

3. Thermal analysis

The formation of the MnNiGe compound was explored using a simultaneous differential scanning calorimeter (DSC) and thermogravimetric analysis device (model: SDT Q600 manufactured by TA instruments, Inc.). The heat flow experiment of MnNiGe SC1100 was performed by sweeping the temperature up to 1100 °C and back to room temperature as shown in figure 2. A first-order phase transition peak due to crystallization/melting was clearly observed around 1000 °C. For those samples with non-magnetic first-order martensitic structural transitions above 400 K, calorimetric experiments were performed to locate their respective transition temperatures with a scanning rate of 2 °C min^{-1} back and forth for multiple cycles. These results along with their corresponding magnetization measurements will be presented in section 4.

4. Magnetization results

Magnetization measurements at ambient pressure and at applied hydrostatic pressure were obtained using a magnetic property measurement system with the reciprocating sample option manufactured by Quantum Design. All iso-field magnetization measurements were executed in a constant magnetic field of $\mu_0 H = 0.1$ T with a scanning rate of 2 K min^{-1} from 100 K to 400 K[5] back and forth for multiple cycles following the conventional field-cooled-warming and field-cooled-cooling protocols.

4.1. Ambient pressure results

The isofield, temperature-dependent magnetization measurement data shown in figure 3 were collected at ambient pressure. First-order martensitic structural transitions with thermal hysteresis characteristics were observed for the quenched samples as well as for the slowly-cooled source sample SC1100, which shows magnetic and structural transitions close to those reported previously [25–27].

The first-order martensitic structural transition temperatures extracted from the temperature-dependent magnetization results and the calorimetric results are tabulated in table 1. Increasing quenching temperatures drastically decreased the

[5] The high-temperature limit of the magnetometer is 400 K.

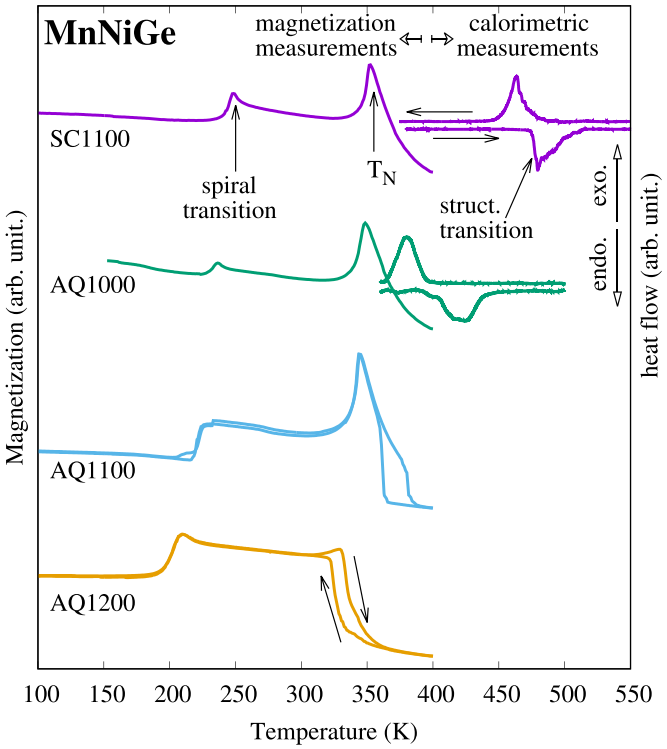

Figure 3. Temperature-dependent magnetization measurements of all MnNiGe samples were performed by following conventional field-cooled-warming and field-cooled-cooling protocols with $\mu_0 H = 0.1$ T. Additional calorimetric experiments were performed for samples SC1100 and AQ1000, and are shown in the upper right side of this figure because their first-order martensitic structural transitions occurred above 400 K. The temperature sweeping directions are denoted by arrows in the magnetization results of sample AQ1200 and calorimetric results of sample SC1100. The first-order martensitic structural transition shifted to lower temperature as the quenching temperatures increased.

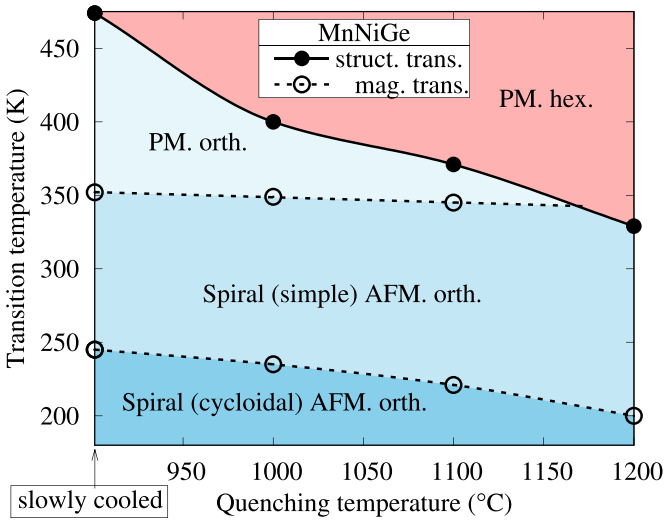

Figure 4. A phase diagram illustrating the relationship between quenching temperatures and transition temperatures in MnNiGe. The first-order martensitic structural transition temperatures are denoted by solid lines, while magnetic transition temperature are shown as dashed lines.

first-order martensitic structural transition temperatures while it concurrently decreased the magnetic transition temperatures of the martensitic phase. When the sample was quenched at 1200 °C, the first-order martensitic structural transition temperature occurred at the lowest temperature (329 K) of all samples. On the other hand, the highest structural transition (474 K) was observed for the sample cooled slowly from 1100 °C. The phase diagram shown in figure 4 summarizes the effects of quenching temperature on both first-order martensitic structural transitions and magnetic transitions based on our experimental results. Although it was not observed here, the complete absence of the first-order martensitic structural transition is expected if a sufficiently high quenching temperature is achieved. In that case, only the Ni_2In-type hexagonal austenite phase would be observed with its second-order magnetic phase transition, similar to those reported in [51–53]. These quenching processes have been commonly applied to obtain metallic materials with reduced long-range atomic ordering [54]. A reduction of long-rang ordering often results in a suppression of magnetic and structural ordering, meaning reduced transition temperatures or the complete elimination of a phase transition [54, 55].

4.2. *Hydrostatic pressures results*

It is known that the structural transition temperatures in MnNiGe prepared by cooling slowly from the melt decrease under hydrostatic pressure [24]. Here, a similar decrease in the structural transition temperature was observed as the quenching temperature increased. To explore this temperature shift phenomenon further, samples AQ1100 and AQ1200 with lower structural transition temperatures were selected for the experiments under hydrostatic pressure. Magnetization measurements under hydrostatic pressure were performed using a commercial BeCu cylindrical pressure cell manufactured by HMD Inc [56, 57]. Daphne 7373 oil was used as the pressure transmitting medium. The magnitude of the applied pressure was calibrated by measuring the shift of the superconducting transition temperature of Sn, which was placed in the cell with the sample.

The temperature-dependent magnetization results for samples AQ1100 and AQ1200, which were measured at ambient pressure and the indicated applied pressures with $\mu_0 H = 0.1$ T, are shown in figure 5. With increasing hydrostatic pressure, the magnetic spiral transitions shifted to higher temperature while the structural transition temperatures decreased. In the pressure range we explored, the linear decreasing rates of the first-order martensitic structural transition temperatures are $-7.1\,\mathrm{K\,kbar^{-1}}$ for samples AQ1100 and $-6.5\,\mathrm{K\,kbar^{-1}}$ for sample AQ1200. Comparable results of the decreasing first-order martensitic structural transition temperatures via pressure application were also observed in Cr-doped and Ti-doped MnNiGe [28–30] as

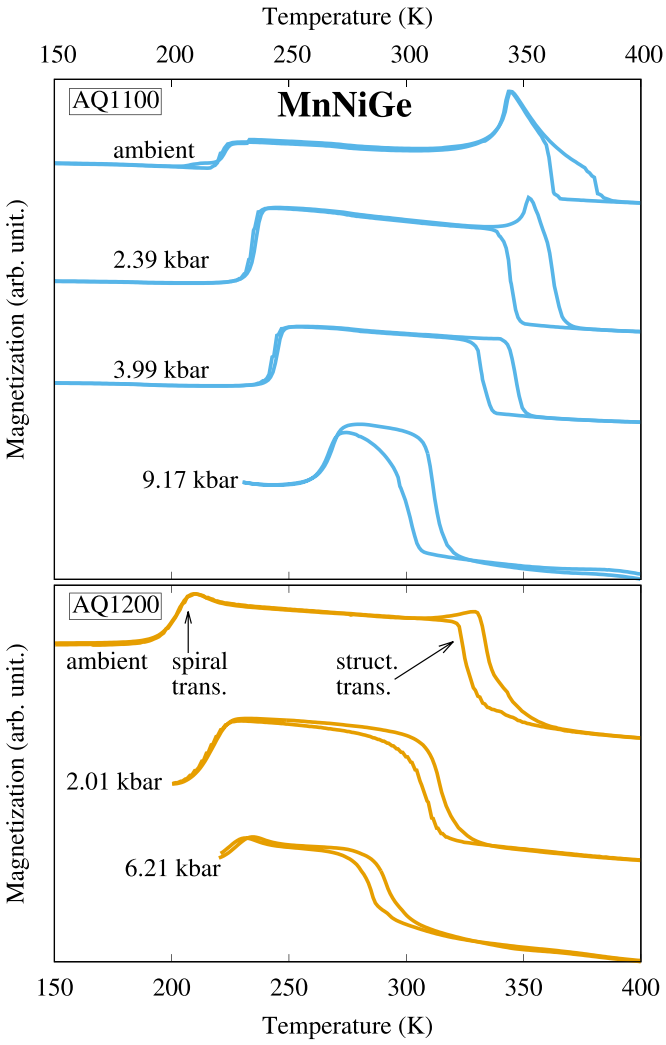

Figure 5. The temperature-dependent magnetization data of MnNiGe samples AQ1100 and AQ1200 measured following conventional field-cooled-warming and field-cooled-cooling protocols at ambient pressure and the indicated applied pressures with $\mu_0 H = 0.1$ T.

Table 2. The rate of decrease of the first-order martensitic structural transition temperatures via pressure application.

Composition	Heat treatment (°C)		Struct. trans. rate (K kbar^{-1})	Reference
MnNiGe	1100	(quenched)	−7.1	this work
MnNiGe	1200	(quenched)	−6.5	this work
MnNiGe	800	(slowly cooled)	−11.1	[24]
$Mn_{0.89}Cr_{0.11}NiGe$	850	(quenched)	−4.6	[28]
$Mn_{0.96}Cr_{0.04}NiGe$	850	(slowly cooled)	−5.3	[29]
$Mn_{0.89}Cr_{0.11}NiGe$	850	(slowly cooled)	−4.6	[29]
$Mn_{0.82}Cr_{0.18}NiGe$	850	(slowly cooled)	−4.8	[29]
$Mn_{0.75}Cr_{0.25}NiGe$	850	(slowly cooled)	−5.3	[29]
$Mn_{0.95}Ti_{0.05}NiGe$	unknown		−5.2	[30]

shown in table 2. The spiral magnetic transition temperatures increased at rates of $+4.8$ K kbar^{-1} for sample AQ1100 and $+3.8$ K kbar^{-1} for sample AQ1200, as illustrated in figure 6. As observed commonly in other Mn*TX* materials which show the martensitic structural transition from a TiNiSi-type orthorhombic to a Ni_2In-type hexagonal [51–53] structure, it is likely that the first-order martensitic transition will no longer occur (i.e. completely disappears) when sufficiently high pressure is applied, or when quenched from sufficiently high temperature.

5. X-ray crystallography

The crystal structures of the MnNiGe samples were identified using powder x-ray diffraction (XRD) measurements, which were performed at the National Synchrotron Radiation

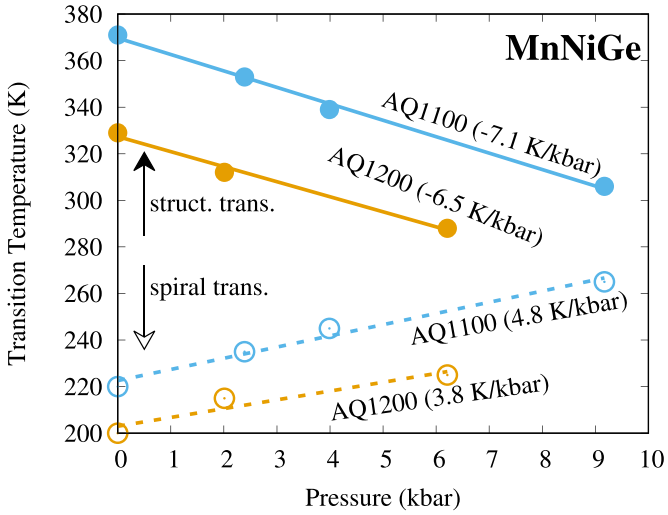

Figure 6. Presure vs. martensitic structural transition temperature and spiral magnetic transition temperature of MnNiGe samples AQ1100 and AQ1200. The rate of change of the structural transition temperatures are $-7.1\,\mathrm{K\,kbar^{-1}}$ for AQ1100 and $-6.5\,\mathrm{K\,kbar^{-1}}$ for AQ1200, whereas those of the spiral magnetic transitions are $+4.8\,\mathrm{K\,kbar^{-1}}$ for AQ1100 and $+3.8\,\mathrm{K\,kbar^{-1}}$ for AQ1200.

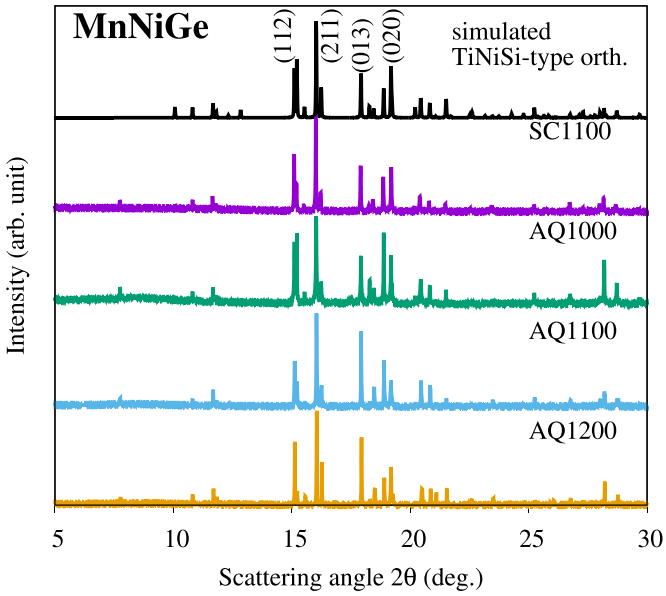

Figure 7. Powder x-ray diffraction results of MnNiGe samples at 100 K for different thermal treatments. The highly crystallographic purity of the TiNiSi-type orthorhombic martensite phase was verified by these results. For comparison, the simulation pattern of the TiNiSi-type orthorhombic structure is shown in the top panel.

Research Center (NSRRC, Taiwan) on beamline TPS-19A with wavelength 0.619 92 Å at $T = 100$ K. To minimize the induced stress due to pulverizing, these samples were thermally cycled across their respective structural transitions repeatedly until they spontaneously fractured into powders [58, 59].

5.1. XRD at 100 Kelvin

The XRD results at $T = 100$ K for all samples in figure 7 confirm the highly crystallographic purity of the TiNiSi-type orthorhombic martensite phase. The respective lattice parameters and cell volumes of the major phases are tabulated in table 1, which were obtained by using general structure analysis system (GSAS) software [60–63]. As the quenching temperature increased, the cell volumes per MnNiGe formula unit decreased. As the volumes decrease, the first-order martensitic structural transition temperatures decrease, which has been commonly observed in Mn*TX*-type materials [51–53] because the Ni_2In-type hexagonal austenite phase is known to have a smaller volume than that of the TiNiSi-type orthorhombic martensite phase.

5.2. XRD across the structural transition

To identify the crystal structure changes across the first-order martensitic structural transitions, we performed temperature-dependent XRD experiments. It is known that the TiNiSi-type orthorhombic martensite phase can be considered as a distortion of the Ni_2In-type hexagonal austenite phase through the relations [23]

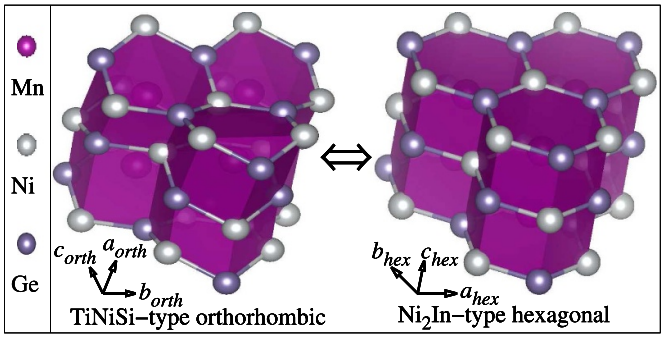

Figure 8. The illustration of the first-order martensitic structural transition between the TiNiSi-type orthorhombic martensite phase and the Ni_2In-type hexagonal austenite phase drawn in a polyhedral view by VESTA [64]. A structural deformation occurs along a_{orth} (i.e. c_{hex}) and b_{orth} (i.e. a_{hex}) during the structural transitions.

$$a_{\mathrm{orth}} \leftrightarrow c_{\mathrm{hex}}$$
$$b_{\mathrm{orth}} \leftrightarrow a_{\mathrm{hex}}$$
$$\text{and } c_{\mathrm{orth}} \leftrightarrow \sqrt{3}a_{\mathrm{hex}}.$$

This distortion is illustrated in figure 8. Based on these transformations, the crystal parameters/volume across the first-order martensitic structural transitions of all the samples are presented in figure 9. As the temperature increased through the structural transitions, a distortion from the low-temperature TiNiSi-type orthorhombic martensite phase to the high-temperature Ni_2In-type hexagonal austenite phase occurred with a 10.4% reduction along a_{orth} and 7.5% expansion along b_{orth}, as shown in figure 9. The changes in cell

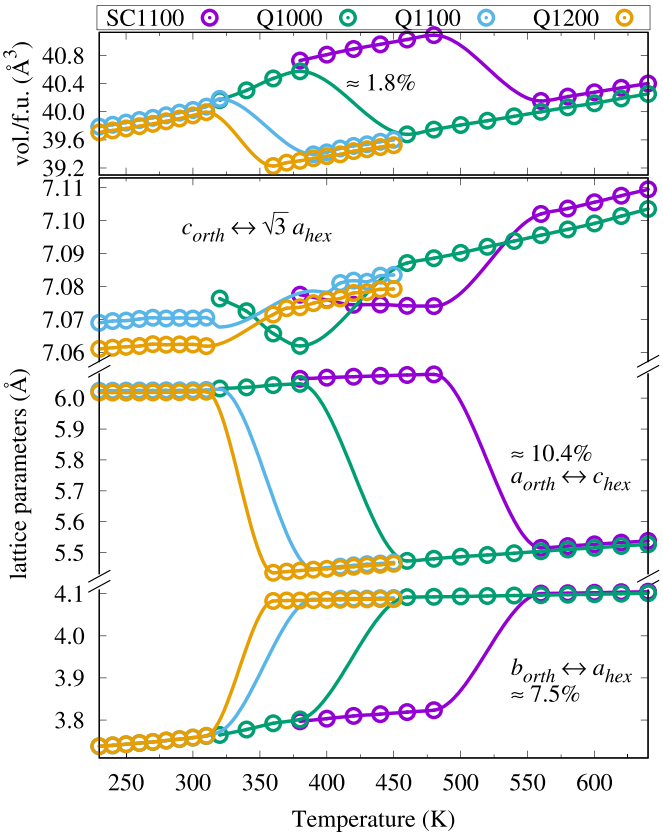

Figure 9. Cell volumes/parameters for all the MnNiGe samples obtained from temperature-dependent XRD. It is observed that the changes in cell parameters/volumes due to the first-order martensitic structural transitions for these four samples remain nearly identical, ≈1.8%, although these structural transitions occurred at different temperatures.

volumes across the first-order martensitic structural transitions for these samples are nearly the same (≈1.8%) although their transition temperatures are significantly separated, comparable to previously reported results [25].

6. Entropy estimate

The total entropy across first-order transitions can be estimated by using the Clausius-Clapeyron relation [65]

$$\Delta S_{0\to P} = \frac{\Delta V}{\Delta T_{\text{struct.}}/\Delta P}$$

if $\Delta T_{\text{struct.}}/\Delta P$ and ΔV are known, where $\Delta T_{\text{struct.}}/\Delta P$ is the rate of change of the first-order martensitic structural transition temperatures with the hydrostatic pressures. The volume changes across the first-order martensitic structural transition are 1.8% from section 5.2 and the linear rates of change of the first-order martensitic structural transition temperatures from section 4.2 are $\Delta T_{\text{struct.}}/\Delta P = -7.1\,\text{K kbar}^{-1}$ (AQ1100), and $-6.5\,\text{K kbar}^{-1}$ (AQ1200). With these experimental results, we found $\Delta S \approx 36\,\text{J}\ (\text{kg}\cdot\text{K})^{-1}$ for sample AQ1100, and $40\,\text{J}\ (\text{kg}\cdot\text{K})^{-1}$ for sample AQ1200. This entropy suggests the possibility of a substantial barocaloric effect (up to $40\,\text{J}\ (\text{kg}\cdot\text{K})^{-1}$) for this sample.

7. Magnetic structures analysis

Previously reported neutron diffraction experiments revealed that slowly-cooled orthorhombic MnNiGe has a simple spiral antiferromagnetic structure at room temperature which transforms to a cycloidal spiral antiferromagnetic structure below 245 K [25, 26, 32, 45, 66, 67]. However, the dependence of these magnetic structures on the synthesis conditions is relatively unknown, such as the effect of quenching, as was applied in the current study. Hence, our quenched sample AQ1200 and slowly-cooled sample SC1100 were chosen to perform time-of-flight experiments on the POWGEN diffractometer at the Spallation Neutron Source, Oak Ridge National Laboratory, USA [68]. The experiments were performed at 300 K and 100 K for these two samples. The experimental results are shown in figure 10 as black circles for samples (a) SC1100 at 300 K, (b) SC1100 at 100 K, (c) AQ1200 at 300 K, and (d) AQ1200 at 100 K.

To determine the nuclear and magnetic structures of the samples, Rietveld refinements were performed using the program FullProf using the conical magnetic model which is commonly used to describe spiral magnetic structures [45, 69, 70], and assuming that only Mn atoms carried magnetic moments. The refinement results are shown in figure 10, in which the circles are observed data, the solid lines are calculated data, the vertical bars represent the Bragg positions of

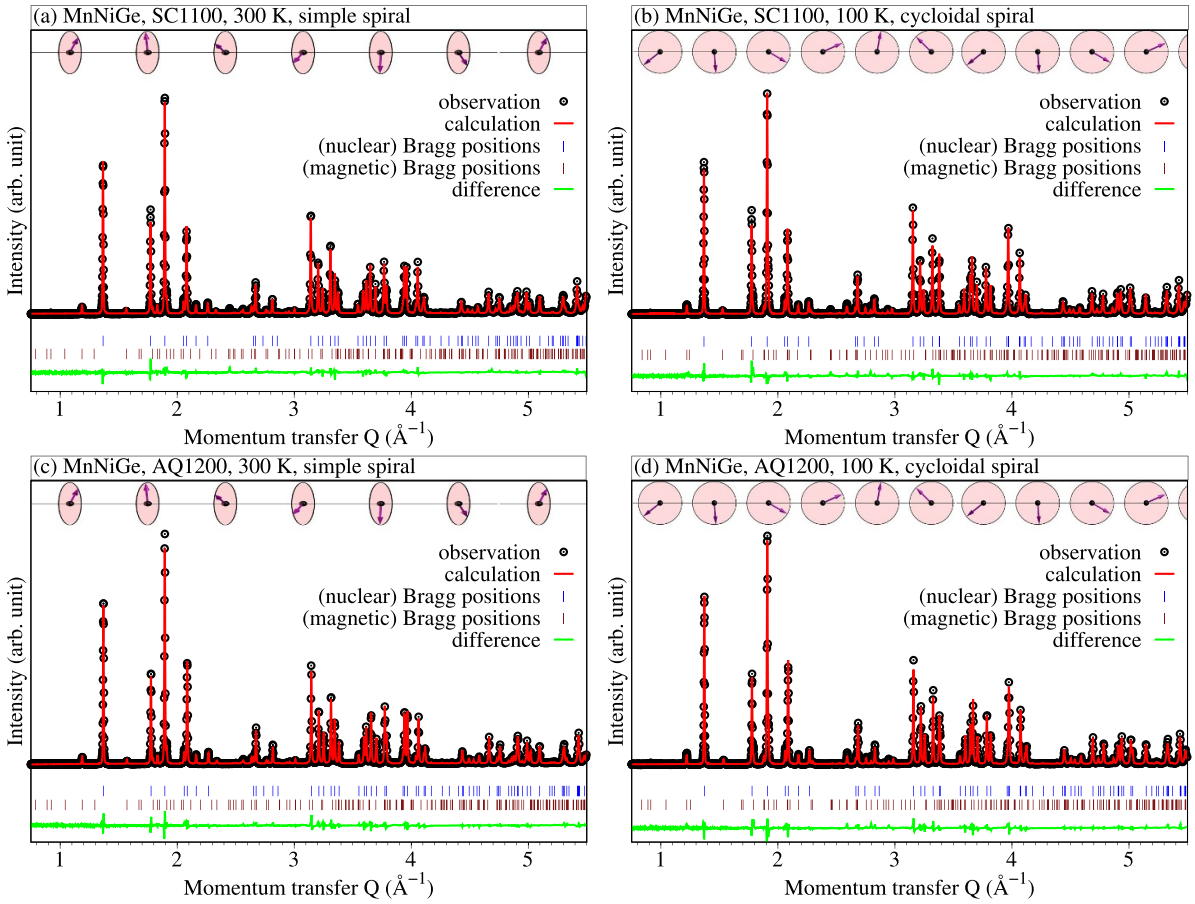

Figure 10. Rietveld refinements of the neutron diffraction patterns for samples (a) SC1100 at 300 K, (b) SC1100 at 100 K, (c) AQ1200 at 300 K, and (d) AQ1200 at 100 K. The black circles and solid red lines are the results from the observation and calculations, respectively. The vertical bars represent the Bragg positions of the proposed nuclear (blue) and magnetic (brown) structures in the orthorhombic martensite phase. The bottom green lines are the differences between observed and calculated data. For all the cases, the propagation vectors along the orthorhombic *a*-axis were found. The refinements suggest a simple spiral antiferromagnetic structure at 300 K and a cycloidal spiral antiferromagnetic structure at 100 K for both samples SC1100 and AQ1200.

their corresponding nuclear and magnetic structures, and the bottom solid lines show the difference between observed and calculated data. The refinement suggest that the propagation vectors were along the orthorhombic *a*-axis regardless of the heat treatments and experimental temperatures. A cycloidal spiral antiferromagnetic structure with the propagation vector $\tau_{\|a_{\mathrm{orth}}} = 0.20$ was found at 100 K for both samples, while a simple spiral antiferromagnetic structure with the propagation vector $\tau_{\|a_{\mathrm{orth}}} = 0.24$ was found at 300 K for both samples. These findings were consistent with other reports [25, 32, 45, 66, 67] for samples prepared through slowly-cooling. Other than the differences of their lattice parameters, no obvious changes of the magnetic structures were observed between the two samples under different heat treatments based on our neutron patterns analysis.

8. Conclusions

The structural and magnetic properties of MnNiGe upon the systematic variation of heat treatment conditions and hydrostatic pressure application were studied. In the sample quenched from 1200 °C, the first-order martensitic structural transition between the TiNiSi-type orthorhombic martensite phase and the Ni_2In-type hexagonal austenite phase decreased drastically (>200 K) compared to the samples that were cooled slowly. As the materials were quenched from higher temperatures, the first-order martensitic structural transition temperatures reduced, and is expected to be completely absent if higher quenching temperatures could be reached. Similarly, as applied hydrostatic pressures increased, the structural transition temperatures decreased linearly by rates up to $-7.1\,\mathrm{K\,kbar^{-1}}$, and presumably for sufficiently high pressures, only the Ni_2In-type hexagonal austenite phase with a second-order magnetic transition will be present. Although the shifts of the phase transition temperatures due to the heat treatment were clearly observed, the neutron scattering results suggest little to negligible effects on their magnetic structures. With respect to possible magnetocaloric applications, our findings demonstrate that the proper heat treatment, pressure application, or both can induce the occurrence of magnetostructural transitions at room temperature. In addition, based on the Clausius-Clapeyron

relation and our experimental results, an entropy change due to the barocaloric effects up to 40 J $(\mathrm{kg}\cdot\mathrm{K})^{-1}$ is possible.

Data availability statement

The data cannot be made publicly available upon publication because they are not available in a format that is sufficiently accessible or reusable by other researchers. The data that support the findings of this study are available upon reasonable request from the authors.

Acknowledgments

S Stadler and J-H Chen acknowledge support from the U.S. Department of Energy, Office of Basic Energy Sciences under Award No. DE-FG02-13ER46946. N Ali and I Dubenko acknowledge support from the U.S. Department of Energy, Office of Basic Energy Sciences under Award No. DE-FG02-06ER46291. D P Young acknowledges support from the U.S. National Science Foundation, Division of Materials Research under Award No. NSF-DMR-1904636. Xiaojian Bai is supported by the Louisiana Board of Regents Support Fund. The DSC data used in this work were collected at the Center for Advanced Microstructures and Devices (CAMD) under the supervision of A Roy. Neutron data were collected at the Spallation Neutron Source, a DOE Office of Science User Facility operated by Oak Ridge National Laboratory.

References

[1] Brück E, Tegus O, Cam Thanh D T, Trung N T and Buschow K H J 2008 *Int. J. Refrig.* **31** 763–70
[2] Brück E 2005 *J. Phys. D: Appl. Phys.* **38** R381
[3] Shen B G, Sun J R, Hu F X, Zhang H W and Cheng Z H 2009 *Adv. Mater.* **21** 4545–64
[4] Gschneidner K A Jr and Pecharsky V K 2008 *Int. J. Refrig.* **31** 945–61
[5] Gschneidner K A Jr, Pecharsky V K and Tsokol A O 2005 *Rep. Prog. Phys.* **68** 1479
[6] Franco V, Blázquez J S, Ingale B and Conde A 2012 *Annu. Rev. Mater. Res.* **42** 305–42
[7] Sandeman K G 2012 *Scr. Mater.* **67** 566–71
[8] Garcia C A C, Bocarsly J D and Seshadri R 2020 *Phys. Rev. Mater.* **4** 024402
[9] Bocarsly J D, Levin E E, Garcia C A C, Schwennicke K, Wilson S D and Seshadri R 2017 *Chem. Mater.* **29** 1613–22
[10] Sun J R, Shen B G and Hu F X 2009 Magnetocaloric effect and materials *Nanoscale Magnetic Materials and Applications* ed J Ping Liu, O Gutfleisch, E Fullerton and D J Sellmyer (Springer) ch 15, pp 472–6
[11] Pecharsky V K and Gschneidner K A Jr 1997 *Phys. Rev. Lett.* **78** 4494–7
[12] Chen J-H, Poudel Chhetri T, Grant A T, Chang C-K, Young D P, Dubenko I, Ali N and Stadler S 2022 *J. Alloys Compd.* **900** 163480
[13] Chen J-H, Bruno N M, Ning Z, Shelton W A, Karaman I, Huang Y, Li J and Ross J H Jr 2018 *J. Alloys Compd.* **744** 785–90
[14] Bruno N M, Yegin C, Karaman I, Chen J-H, Ross J H Jr. Liu J and Li J 2014 *Acta Mater.* **74** 66–84
[15] Chen J-H, Bruno N M, Karaman I, Huang Y, Li J and Ross J H Jr 2014 *J. Appl. Phys.* **116** 203901
[16] Huang Y, Hu Q, Bruno N, Chen J-H, Karaman I, Ross J H Jr and Li J 2015 *Scr. Mater.* **105** 42–45
[17] Sutou Y, Imano Y, Koeda N, Omori T, Kainuma R, Ishida K and Oikawa K 2004 *Appl. Phys. Lett.* **85** 4358–60
[18] Krenke T, Duman E, Acet M, Wassermann E F, Moya X, Mañosa L and Planes A 2005 *Nat. Mater.* **4** 450–4
[19] Khan M, Ali N and Stadler S 2007 *J. Appl. Phys.* **101** 053919
[20] Liu F S, Wang Q B, Ao W Q, Yu Y J, Pan L C and Li J Q 2012 *J. Magn. Magn. Mater.* **324** 514–8
[21] Krenke T, Duman E, Acet M, Wassermann E F, Moya X, Mañosa L, Planes A, Suard E and Ouladdiaf B 2007 *Phys. Rev.* B **75** 104414
[22] Chen J-H, Bruno N M, Karaman I, Huang Y, Li J and Ross J H Jr 2016 *Acta Mater.* **105** 176–81
[23] Johnson V 1975 *Inorg. Chem.* **14** 1117–20
[24] Anzai S and Ozawa K 1978 *Phys. Rev.* B **18** 2173–8
[25] Bażela W, Szytuła A, Todorović J, Tomkowicz Z and Zikeba A 1976 *Phys. Status Solidi* a **38** 721–9
[26] Fjellvåg H and Andresen A F 1985 *J. Magn. Magn. Mater.* **50** 291–7
[27] Nizioł S, Wesełucha A, Bażela W and Szytuła A 1981 *Solid State Commun.* **39** 1081–5
[28] Jaworska-Gołąb T, Baran S, Duraj R, Marzec M, Dyakonov V, Sivachenko A, Tyvanchuk Y, Szymczak H and Szytuła A 2015 *J. Magn. Magn. Mater.* **385** 1–6
[29] Duraj R, Szytuła A, Jaworska-Gołąb T, Deptuch A, Tyvanchuk Y, Sivachenko A, Val'kov V and Dyakonov V 2018 *J. Alloys Compd.* **741** 449–53
[30] Duraj R, Zach R and Szytuła A 1988 *J. Magn. Magn. Mater.* **73** 69–78
[31] Szytuła A *et al* 2017 *J. Alloys Compd.* **726** 978–88
[32] Penc B, Hoser A, Baran S and Szytuła A 2018 *Phase Transit.* **91** 118–27
[33] Penc B *et al* 2018 *Phase Transit.* **91** 1107–21
[34] Zubov E *et al* 2018 *Low Temp. Phys.* **44** 775–9
[35] Rimskii G, Yanushkevich K, Belozerova N, Kozlenko D and Rutkauskas A 2021 *Phys. Solid State* **63** 485–91
[36] Ito M, Onda K, Kashima R, Matsuo A and Kindo K 2022 *J. Magn. Magn. Mater.* **546** 168767
[37] Roy R, Adhikari S K, Sannigrahi J, Mandal K, Das S C, Dutta P, Pramanick S, Khalyavin D, Adroja D T and Chatterjee S 2021 *Phys. Rev.* B **104** 214405
[38] Zhou H *et al* 2022 *J. Mater. Sci. Technol.* **114** 73–80
[39] Dutta P, Pramanick S, Singh V, Major D T, Das D and Chatterjee S 2016 *Phys. Rev.* B **93** 134408
[40] Poudel Chhetri T, Chen J-H, Grant A T, Young D P, Dubenko I, Talapatra S, Ali N and Stadler S 2022 *J. Appl. Phys.* **132** 045107
[41] Poudel Chhetri T, Chen J-H, Grant A T, Young D P, Dubenko I, Talapatra S, Ali N and Stadler S 2023 *J. Appl. Phys.* **133** 065104
[42] Mandal K, Das S, Dutta P, Pramanick S and Chatterjee S 2020 *J. Alloys Compd.* **822** 153454
[43] Yang H, Liu J, Li C, Wang G-L, Gong Y-Y and Xu F 2018 *Chin. Phys.* B **27** 107502
[44] Mandal K, Dutta P, Dasgupta P, Pramanick S and Chatterjee S 2018 *J. Phys. D: Appl. Phys.* **51** 225004
[45] Ren Q, Hutchison W D, Wang J, Studer A J and Campbell S J 2018 *Chem. Mater.* **30** 1324–34
[46] Zhu F *et al* 2020 *J. Alloys Compd.* **820** 153151
[47] Das S C, Sannigrahi J, Dutta P, Pramanick S, Khalyavin D, Adroja D T and Chatterjee S 2021 *Phys. Rev.* B **103** 094422
[48] You J and Guo Y 2019 *Mater. Lett.* **239** 172–5
[49] Zhang C L, Wang D H, Cao Q Q, Han Z D, Xuan H C and Du Y W 2008 *Appl. Phys. Lett.* **93** 122505

[50] Daniel-Pérez G, Sánchez Llamazares J L, Quintana-Nedelcos A, Álvarez Alonso P, Varga R and Chernenko V 2014 *J. Appl. Phys.* **115** 17A920
[51] Chen J-H, Poudel Chhetri T, Chang C-K, Huang Y-C, Young D P, Dubenko I, Talapatra S, Ali N and Stadler S 2021 *J. Appl. Phys.* **129** 215108
[52] Chen J-H, Us Saleheen A, Karna S K, Young D P, Dubenko I, Ali N and Stadler S 2018 *J. Appl. Phys.* **124** 203903
[53] Chen J-H, Poudel Chhetri T, Us Saleheen A, Young D P, Dubenko I, Ali N and Stadler S 2019 *Intermetallics* **112** 106547
[54] Luborsky F 1983 Amorphous metallic alloys *Amorphous Metallic Alloys* ed F E Luborsky (Butterworth-Heinemann) ch 1, pp 1–7
[55] O'Handley R 1983 Fundamental magnetic properties *Amorphous Metallic Alloys* ed F E Luborsky (Butterworth-Heinemann) ch 14, pp 257–82
[56] Mito M and Hamada M 2014 *US Patent* 8,789456 B2 Piston cylinder-type high-pressure generating device
[57] Mito M 2007 *J. Phys. Soc. Japan* **76** 182–5
[58] Samanta T *et al* 2015 *J. Appl. Phys.* **117** 123911
[59] Samanta T *et al* 2015 *Phys. Rev.* B **91** 020401(R)
[60] Larson A C and Von Dreele R B 2004 General structure analysis system (GSAS) *Report* LAUR 86–748 (Los Alamos National Laboratory)
[61] Toby B H 2001 *J. Appl. Crystallogr.* **34** 210
[62] Hammond C 2009 *The Basics of Crystallography and Diffraction* (*International Union of Crystallography Texts on Crystallography*) 3rd edn (Oxford University Press)
[63] Pecharsky V K and Zavalij P Y 2009 *Fundamentals of Powder Diffraction and Structural Characterization of Materials* 2nd edn (Springer)
[64] Momma K and Izumi F 2011 *J. Appl. Crystallogr.* **44** 1272–6
[65] Huang K 1987 *Statistical Mechanics* (Wiley)
[66] Bażela W, Szytuła A, Todorović J and Zikęba A 1981 *Phys. Status Solidi* a **64** 367–78
[67] Nizioł S, Bombik A, Bażela W, Szytuła A and Fruchart D 1982 *J. Magn. Magn. Mater.* **27** 281–92
[68] Huq A, Kirkham M, Peterson P F, Hodges J P, Whitfield P S, Page K, Hugle T, Iverson E B, Parizzi A and Rennich G 2019 *J. Appl. Crystallogr.* **52** 1189–201
[69] Rodríguez-Carvajal J 1993 *Physica* B **192** 55–69
[70] Rodríguez-Carvajal J and Bourée F 2012 *EPJ Web Conf.* **22** 00010